Nanoscale Horizons

ROYAL SOCIETY OF CHEMISTRY

COMMUNICATION

View Article Online
View Journal | View Issue

Cite this: *Nanoscale Horiz.*, 2025, **10**, 2374

Received 21st May 2025,
Accepted 18th July 2025

DOI: 10.1039/d5nh00358j

rsc.li/nanoscale-horizons

Surface ligand networking promotes intersystem crossing in the $Au_{18}(SR)_{14}$ nanocluster†

Guiying He,[a] Zhongyu Liu,[a] Yitong Wang,[a] Matthew Y. Sfeir[bc] and Rongchao Jin*[a]

Understanding the relationships between the structure and optical properties of ligand-protected, atomically precise metal nanoclusters (NCs) is of paramount importance for exploring their applications in photonics, biomedicine and quantum technology. Here, two $Au_{18}(SR)_{14}$ NCs protected by 2,4-dimethylbenzenethiolate (DMBT) and cyclohexanethiolate (CHT), respectively, are studied using time-resolved absorption and emission spectroscopies. Although the two NCs exhibit similar photoluminescence (PL) quantum yields (QY ~ 0.1%) at room temperature, their excited state dynamics are very different, which are modulated by the interactions between the Au core and the ligands, as well as the networking interactions among aromatic ligands. Specifically, $Au_{18}(CHT)_{14}$ exhibits a single exponential decay of its singlet excited state (time constant τ = 17 ns) with almost no triplet population. In contrast, there is a triplet population of more than 15% for $Au_{18}(DMBT)_{14}$, and an intersystem crossing (ISC) process of ~4 ns is identified. Temperature-dependent PL measurements of $Au_{18}(DMBT)_{14}$ show three radiative processes, including prompt fluorescence, thermally activated delayed fluorescence and phosphorescence. The non-radiative process is partially suppressed at low temperatures, leading to enhanced photoluminescence (QY up to 9.0%) and exclusive phosphorescence was observed below 120 K. The obtained insights into the excited state energy flow and PL dynamics will benefit future design of luminescent NCs for optoelectronic applications.

New concepts

Research on atomically precise nanoclusters (APNCs) of metals and alloys in the past years has led to a rich library of APNCs with atomic structures determined by X-ray crystallography. The current thrust is to understand the rich functionality of APNCs, in particular, the structure–function correlation for their unique near-infrared (NIR, *e.g.* 800–2000 nm wavelengths) luminescence. Many concepts remain to be explored, such as the electron–vibration coupling and excited state control. In this work, we are motivated to understand the ultrafast excited state energy flow and how it can be directed toward the NIR luminescence. While quantum theory has coined spin–orbit coupling and singlet–triplet energy gap as two important factors that govern the intersystem crossing (ISC), other important factors remain to be discovered experimentally. Our work recognizes for the first time that the surface ligands' networking interactions can have a large influence on the ISC kinetics. This conceptual advance may add a new dimension to the tailoring of the ISC process toward the construction of strongly luminescent APNCs for optoelectronic applications as well as quantum technology (*e.g.* APNCs as single photon emitters).

Introduction

Atomically precise metal nanoclusters (NCs) have emerged as a new class of materials, which provide a great opportunity to study the structure–function relationships at the atomic level.[1,2] With ligand protection, metal NCs can be stabilized and crystallized for atomic structure determination.[3–5] The past decade has witnessed significant progress in thiolate-protected metal NCs because of their high stability and wide applications

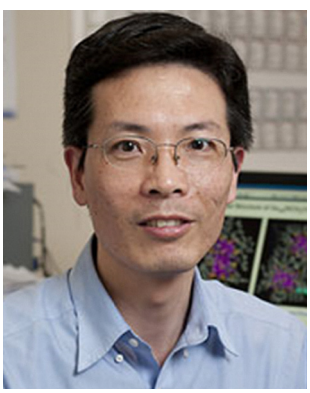

Rongchao Jin

Congratulations on the 10th anniversary of Nanoscale Horizons and its being at the forefront of nanoscience for a decade! It is my pleasure to serve on the Advisory Board of Nanoscale Horizons and to have observed the journal's steady growth over the years. On this special occasion, my coworkers and I are excited to make a contribution for the celebration. We would like to extend our best wishes for the promise of the journal's next decade to lead nanoscience research!

[a] *Department of Chemistry, Carnegie Mellon University, Pittsburgh, Pennsylvania 15213, USA. E-mail: rongchao@andrew.cmu.edu*
[b] *Department of Physics, Graduate Center, City University of New York, New York, NY 10016, USA*
[c] *Photonics Initiative, Advanced Science Research Center, City University of New York, New York, NY 10031, USA*

† Electronic supplementary information (ESI) available. See DOI: https://doi.org/10.1039/d5nh00358j

in bioimaging, photocatalysis, solar cells, *etc.*[6–13] Luminescent metal NCs are of special interest because of their low toxicity, large Stokes shift, and long luminescence lifetime.[14,15] To enhance the photoluminescence (PL) properties, it is essential to understand the PL mechanism, which is related to the NC size,[16–19] shape,[20–22] surface structure and core structures.[23–33]

The inner gold kernel (core) and surface motifs (shell) of thiolate-protected Au nanoclusters are both important contributors to their unique PL properties in the near-infrared (NIR) wavelength window.[34–39] Experimental and theoretical research revealed the ultrafast electron dynamics and PL mechanism with core-to-shell relaxation.[40–45] Considering the coupling between the core and the shell, the individual roles of these two intertwined structural parameters have been studied in the case of $Au_{28}(SR)_{20}$ quasi-isomers which share the same core but different shell structures.[16] Specifically, the rigid structure of $Au_{28}(CHT)_{20}$ exhibits more than 15-fold higher PL quantum yield than $Au_{28}(TBBT)_{20}$.[16] In addition, the isomeric effect of $Au_{28}(CHT)_{20}$ was also demonstrated as a key factor in the excited state dynamics related to the singlet and triplet states.[46] Furthermore, the effects of ligand types (thiol *vs.* alkyne) were studied to unveil the catalytic and luminescence mechanisms even though it is difficult to obtain such isostructural NCs.[39,47–49] Wang's group reported that the photoluminescence quantum yield (QY) of alkynyl-protected Au_{28} was 10 times higher than that of the thiolate-protected counterpart,[50] which indicates a significant effect of the ligand type on the luminescence. Recently, we reported the NIR emission of thiolate-protected $Au_{18}(DMBT)_{14}$ and $Au_{18}(CHT)_{14}$ with QY ~ 0.1%. Interestingly, after coating the Au_{18} NCs with an amphiphilic polymer, their PLQY was enhanced by 10 times (up to 1%) without changing the emission peak wavelength.[51] Stamplecoskie *et al.* previously investigated the ultrafast electron relaxation dynamics of glutathione-protected $Au_{18}(SG)_{14}$ in aqueous solution, and the PL of $Au_{18}(SG)_{14}$ was determined to be 6.8% by a relative method, much higher than that of $Au_{18}(CHT)_{14}$ (0.09%).[52] The Au_{18} PL properties have also been investigated by other groups,[53–58] including ensemble and single cluster studies.[58] To explore the unique NIR emission of Au NCs, it is critically important to gain a fundamental understanding of the excited state dynamics.[40–45,52] There have been indications that Au NCs possess quite unusual excited state dynamics,[4,40,43,52] but research on the excited state and PL dynamics is still quite limited.[58]

In this work, we study the intricate excited state dynamics of $Au_{18}(SR)_{14}$ NCs by time-resolved spectroscopy and reveal the surprising ligand effects in the isostructural pair of $Au_{18}(DMBT)_{14}$ and $Au_{18}(CHT)_{14}$. The PL dynamics of $Au_{18}(CHT)_{14}$ indicate a single decay of 17 ns from the lowest singlet excited state, but $Au_{18}(DMBT)_{14}$ exhibits two components in PL dynamics, including a fast decay of ~4 ns and a long-lived one (>100 ns). Transient absorption results indicate a long-lived species lasting up to 180 ns for $Au_{18}(DMBT)_{14}$, which should be attributed to the triplet state. Thus, the fast decay is ascribed to intersystem crossing (ISC). The intricate PL mechanism of $Au_{18}(DMBT)_{14}$ is further probed by temperature-dependent PL measurements. Overall, there are three emission channels related to the interplay of singlet and triplet states: prompt fluorescence (FL), thermally activated delay fluorescence (TADF) and phosphorescence (PH). The PLQY is enhanced by suppression of nonradiative processes at low temperatures. Additionally, only phosphorescence remains

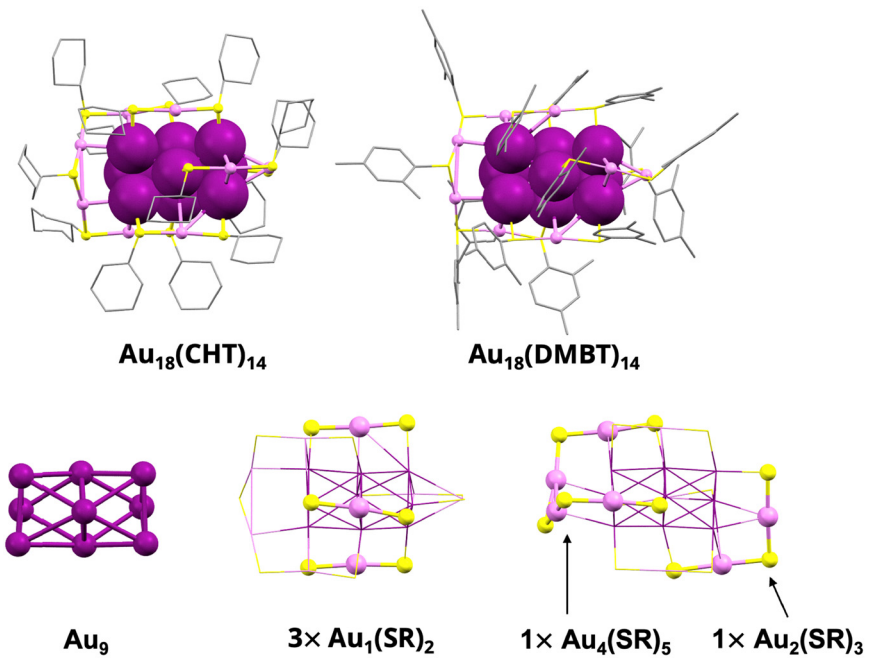

Scheme 1 Atomic structures of $Au_{18}(CHT)_{14}$ and $Au_{18}(DMBT)_{14}$ nanoclusters. Color code: purple, pink: gold; yellow: sulfur; gray: carbon. Hydrogen atoms are omitted for clarity.

when the temperature is lower than 120 K. The obtained insights into the excited state dynamics and PL mechanism will benefit the development of NC-based functional materials with high luminescence for optoelectronics and other applications.

Results and discussion

The synthesis of $Au_{18}(DMBT)_{14}$ followed our recent work,[51] and $Au_{18}(CHT)_{14}$ was earlier reported.[59] X-ray structures of both $Au_{18}(CHT)_{14}$ and $Au_{18}(DMBT)_{14}$ possess a hexagonal close-packed Au_9 rod kernel in a $Au_3/Au_3/Au_3$ tri-layer packing (Scheme 1), and the kernel is protected on its sides by three monomeric $Au(SR)_2$ staple motifs and at its ends by one tetrameric $Au_4(SR)_5$ and one dimeric $Au_2(SR)_3$ staple motif, respectively.[51,59,60] Although the $Au_{18}S_{14}$ frameworks are similar, the structure of $Au_{18}(DMBT)_{14}$ differs from that of $Au_{18}(CHT)_{14}$ in the surface –R groups and the arrangements. For the latter aspect, the aromatic DMBT ligands exhibit inter-ligand $\pi\cdots\pi$ stacking and C–H$\cdots\pi$ interactions, and such networking interactions help to enhance the shielding effect and block external attacks, hence, leading to much higher stability of $Au_{18}(DMBT)_{14}$.[51] Such supramolecular interactions were also reported in the case of $Au_{25}(SR)_{18}$ with surface ligand networking-directed assembly into supercrystals.[61]

The UV-vis spectra of $Au_{18}(DMBT)_{14}$ and $Au_{18}(CHT)_{14}$ are shown in Fig. 1a for comparison. From 300 to 800 nm wavelength, $Au_{18}(CHT)_{14}$ shows four absorption bands at 325, 453, 570, and 630 nm (Fig. 1a, yellow dashed line), whereas $Au_{18}(DMBT)_{14}$ shows redshifted and less prominent bands at 345, 472, 620, and 670 nm (Fig. 1a, cyan dashed line), with the 670 nm band being much less pronounced (*i.e.*, a hump). In previous work on $Au_{18}(CHT)_{14}$, the calculated absorption spectrum of $Au_{18}(SR)_{14}$ by time-dependent density functional theory (TD-DFT) indicated that the HOMO to HOMO−20 were mainly composed of the Au(5d) atomic orbitals and the unoccupied orbitals were sp-band owing to the contribution of Au(6sp) atomic orbitals.[59,60,62] The redshifted and broadened absorption of $Au_{18}(DMBT)_{14}$ compared to $Au_{18}(CHT)_{14}$ is induced by the stronger electronic interaction between the Au core and the aromatic DMBT, that is, electron delocalization. The differences between the two NCs suggest that the electronic structure is modulated by the surface organic ligands, especially the conjugated DMBT ligand compared to the nonaromatic CHT ligand. Both NCs possess a charge transfer (CT) component in their electronic transitions according to the TD-DFT simulations, and the CT process is from the core to the staples.[59]

The two $Au_{18}(SR)_{14}$ NCs show weak near-infrared (NIR) photoluminescence (QY ~ 0.1%),[51,52,58] thus, the non-radiative process constitutes the main decay channel of excited states.[39,58,62–65] An emission peak at 870 nm was observed for both $Au_{18}(SR)_{14}$ NCs (Fig. 1a). In addition, the photoluminescence of $Au_{18}(DMBT)_{14}$ shows a red tail (centered at ~1050 nm) compared to $Au_{18}(CHT)_{14}$, which indicates a complicated emission mechanism (*vide infra*).

The PL dynamics was investigated by a time-correlated single photon counting (TCSPC) technique. We first focus on the early time decay (up to 50 ns range) to obtain high time-resolution (sub-nanosecond) as shown in Fig. 1b. The single exponential fitting worked for the PL decay of $Au_{18}(CHT)_{14}$; thus, it possesses only one PL lifetime (τ = 17 ns), which should be attributed to the decay of the first singlet excited state (S_1), including radiative and nonradiative processes. The population of the long-lived state in $Au_{18}(CHT)_{14}$ is less than 5%, and is hence considered negligible. In contrast, bi-exponential fitting is required for $Au_{18}(DMBT)_{14}$, which gives rise to two lifetime components: τ_1 = 4 ns (85% relative amplitude, *i.e.* photon percentage) and τ_2 = 120 ns (15% relative amplitude). We tentatively assign the emission from S_1 and the first triplet state (T_1), and the ISC process occurs at around 4 ns, which competes with the S_1 radiative decay. In this picture, S_1 and T_1 energies are very close, resulting in a single overall emission peak without splitting, which has been observed in other NCs. The details of the radiative process related to the triplet state will be discussed in the temperature-dependent FL measurements below.

To gain a deeper understanding of the origin of their weak photoluminescence and electron dynamics, we performed femto- and nano-second transient absorption spectroscopies (fs- and ns-TA) on the two $Au_{18}(SR)_{14}$ NCs. Previous work indicates broad excited state signals; thus, we performed fs-TA and ns-TA analyses in both visible and NIR regions. As

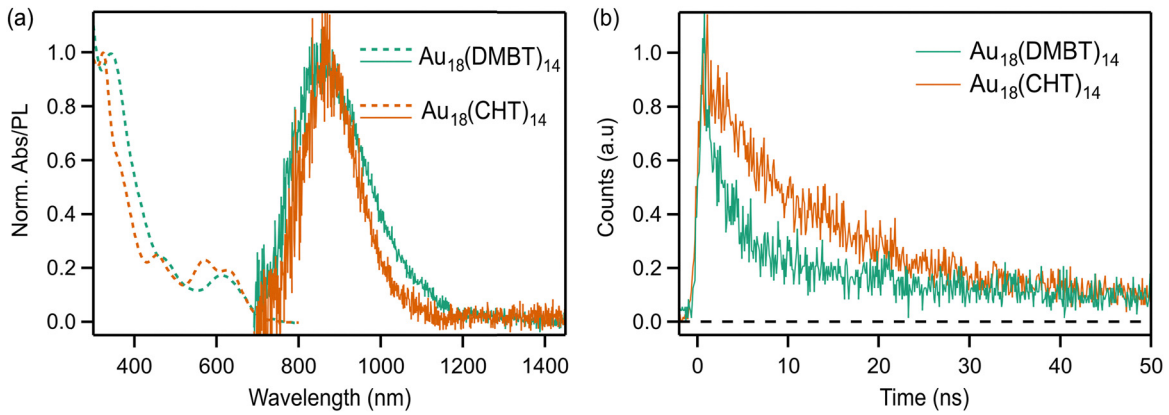

Fig. 1 Steady-state optical absorption and photoluminescence spectra (a) and the photoluminescence lifetimes (b) of the two $Au_{18}(SR)_{14}$ NCs with different –R groups.

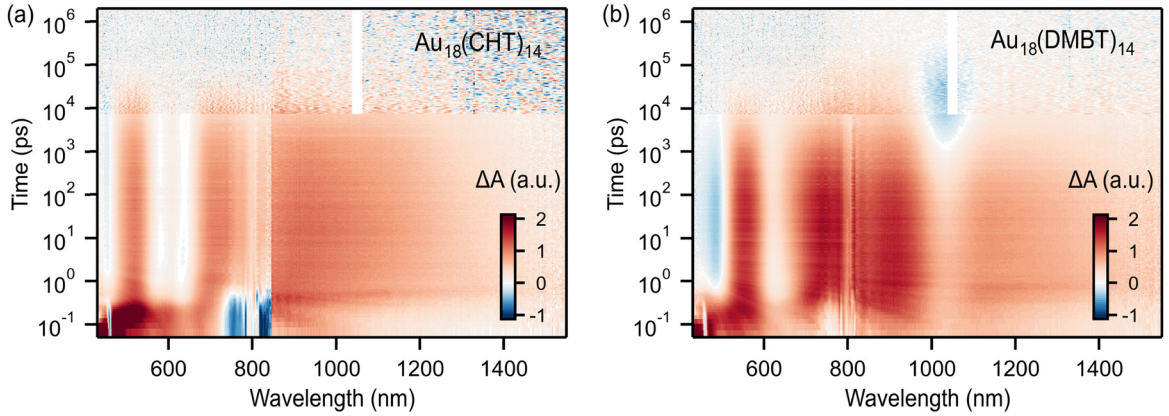

Fig. 2 Transient absorption data maps of (a) $Au_{18}(CHT)_{14}$ and (b) $Au_{18}(DMBT)_{14}$. The NCs were dissolved in toluene and excited at 400 nm, and each of the 2D data maps is composed of the fs-TA (lower part, <7 ns) and the ns-TA (upper part).

shown in Fig. 2, after excitation with a 400 nm pulse, $Au_{18}(CHT)_{14}$ exhibits very broad excited state absorption (ESA) spanning the visible and NIR regions, along with ground state bleaching (GSB) signals at 450, 570 and 630 nm (Fig. 2a), whereas $Au_{18}(DMBT)_{14}$ shows GSB signals at 480 and 630 nm, which are consistent with their steady-state absorption spectra. While the NIR region comprises ESA signals for both $Au_{18}(SR)_{14}$ NCs, it should be noted that a negative signal at 1030 nm for $Au_{18}(DMBT)_{14}$ was observed (Fig. 2b), which is beyond the steady-state absorption region (<700 nm). As the 1030 nm signal from $Au_{18}(DMBT)_{14}$ falls in the emission region (*cf*, Fig. 1a), it indicates that this signal is a stimulated emission (SE), which is rarely observed in the NCs.

The ns-TA data indicate that $Au_{18}(CHT)_{14}$ exhibits only the decay of one excited-state species with the excited state lifetime of 16.7 ns (Fig. S1, ESI†), which is identical to the PL lifetime (17 ns) from the singlet state. We did not observe any obvious long-lived triplet state. In contrast, the excited state kinetics of $Au_{18}(DMBT)_{14}$ indicate both a short decay (4.4 ns) and a long one (181 ns), see Fig. S2 (ESI†). We attribute the first process to the ISC process, similar to the assignment of the results from PL dynamics, and the second one to the decay of the triplet state. These two lifetime components are consistent with the results (τ_1 = 4 and τ_2 = 120 ns) from the TCSPC measurements.

Further fs-TA analysis was employed to investigate the ultrafast excited state dynamics of $Au_{18}(SR)_{14}$. The time constants from ns-TA analysis were fixed and fed into the fs-TA data fitting to extract the ultrafast processes (Fig. 3). The results were verified by kinetics fitting of selecting wavelengths (see Fig. S3–S6, ESI†). We obtained state-resolved relaxation associated with multiple excited states. After excitation at 400 nm, one can observe an ultrafast decay during the first picosecond for both Au_{18} NCs, which is the ultrafast internal conversion (IC) process ($S_n \rightarrow S_1$).[16,52,63] An intermediate lifetime on the order of hundreds of picoseconds was also found, which should be the equilibration to the emissive state.[52,64] Specifically, the time constant of 245 ps for $Au_{18}(DMBT)_{14}$ may be ascribed to the structural relaxation with charge transfer properties. Similarly, the structural relaxation time was 318 ps for $Au_{18}(CHT)_{14}$. Since there is no observed vibronic structure in the absorption spectrum and a redshift of the emission spectrum, more CT character is expected for $Au_{18}(DMBT)_{14}$ compared to $Au_{18}(CHT)_{14}$. This CT is a nonradiative process and contributes to the loss of excitation energy. Given the fact that weak emission is observed from both $Au_{18}(SR)_{14}$, we believe that

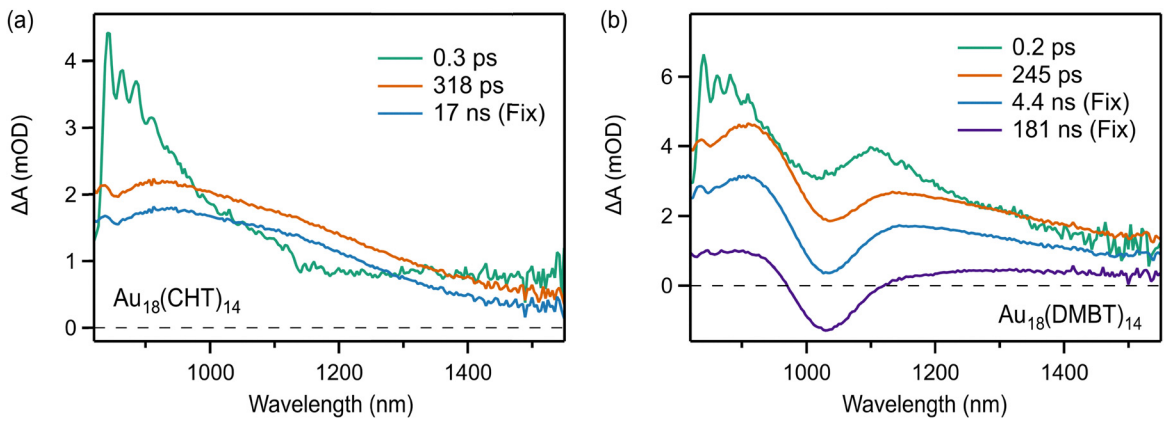

Fig. 3 Global analysis of fs-TA data of (a) $Au_{18}(CHT)_{14}$ and (b) $Au_{18}(DMBT)_{14}$ in the NIR region.

the structural relaxation state (S_{CT}, a singlet state) is less radiative than the S_1 state.

The above results indicate quite complicated dynamics occurring in $Au_{18}(DMBT)_{14}$, which may be related to the interplay between the singlet and triplet states. The rigid protecting-shell by ligand networking can mediate the intersystem crossing process by adjusting the energy level alignment of singlet and triplet states. Considering the increased triplet population of $Au_{18}(DMBT)_{14}$ than the case of $Au_{18}(CHT)_{14}$, we measured temperature-dependent steady state PL spectra and dynamics down to 80 K to determine the radiative process by suppressing the nonradiative process. The $Au_{18}(DMBT)_{14}$ NC was dissolved in 2-methyltetrahydrofuran (2-MeTHF), which can form clear "glass" at cryogenic temperatures for optical measurements. As shown in Fig. 4a, the PL peak becomes sharper and blue-shifted as the temperature decreases. The full width at half maximum (FWHM) was 190 nm at room temperature but narrows down to 90 nm at 80 K (see normalized PL spectra in Fig. S7, ESI†). The integrated intensity of the PL peak increases monotonically from room temperature to 80 K, in which the PLQY is increased to 9.0% at 80 K. Note that when the temperature is higher than 200 K, the emission peak remains at around 860 nm (Fig. S8, ESI†). When decreasing from 200 K, the emission peak starts to blue shift and becomes more rapid when the temperature is below 120 K. Finally, the emission peak is blue-shifted to 795 nm at 80 K (Fig. S8, ESI†). A similar trend was observed for PLQY (Fig. S9, ESI†).

We extended the PL lifetime measurements (Fig. 4b) to microseconds in order to detect the emission related to the triplet state, including phosphorescence and/or thermally activated delayed fluorescence (TADF).[17,31,46,65,66] Table 1 summarizes the PL kinetics fitting and QY of $Au_{18}(DMBT)_{14}$. We attribute τ_2 to the lifetime of TADF and τ_3 to the phosphorescence. The shortest time constant τ_1 ~10 ns, which should stem from radiative relaxation of the first singlet state (S_1) but is not exact due to the large time steps in the measurements (2.5 ns per step for a measurement range of 5 μs and 25 ns per step for 50 μs). The longest time constant (τ_3), 0.7 μs at 280 K to 7.6 μs at 80 K, is from the radiative relaxation of the triplet state T_1. As the temperature decreases from room temperature down to 120 K, τ_2 and τ_3 become longer and the percentage of τ_3 increases rapidly, while the percentages of τ_1 and τ_2 decrease (Table 1), implying a process of population transfer between the states (*i.e.* reverse intersystem crossing, RISC). Interestingly, when the temperature is lower than 120 K, only one component (τ_3) remains, whereas the other radiative processes are completely suppressed. Generally, TADF *via* RISC dictates a very small gap between S_1 and T_1 (*e.g.* <0.2 eV).[31] When the temperature was down to 120 K, the RISC process for $Au_{18}(DMBT)_{14}$ was suppressed completely.

Table 1 PL lifetime components, relative amplitudes (%), and QY of $Au_{18}(DMBT)_{14}$ at different temperatures by multi-exponential fitting the TCSPC data in Fig. 4b

Temperature	τ_1 (ns)	τ_2 (ns)	τ_3 (μs)	QY (%)
80 K	—	—	7.6 (100%)	9.0
100 K	—	—	6.5 (100%)	5.6
120 K	12 (37%)	293 (22%)	3.9 (41%)	4.7
140 K	16 (42%)	275 (11%)	3.3 (47%)	3.7
160 K	7.8 (38%)	439 (14%)	2.4 (48%)	3.6
180 K	11 (30%)	289 (32%)	2.3 (38%)	2.1
200 K	6.3 (41%)	158 (28%)	1.9 (31%)	1.3
220 K	15 (44%)	200 (23%)	1.4 (33%)	0.58
240 K	14 (52%)	205 (24%)	0.99 (23%)	0.31
260 K	7 (54%)	117 (31%)	0.77 (15%)	0.18
280 K	11 (52%)	113 (37%)	0.78 (11%)	0.15

Based on the above results, we propose the excited state dynamics of $Au_{18}(DMBT)_{14}$ as shown in Fig. 5. At room temperature, the emission stems from fluorescence, TADF and phosphorescence, which contribute to the PL spectra and time-resolved measurements. The emissive states are closely spaced; thus, the PL shows an overall single peak without splitting. The relaxation component ($S_1 \rightarrow S_{CT}$) is on the order of hundreds of ps from the fs-TA measurements. The relaxation of S_{CT} (4 ns) includes both radiative decay to the ground state and ISC to the triplet state. The triplet state lifetime increases with decreasing temperature (up to 7.6 μs at 80 K), along with the enhancement of QY. As the temperature goes down, the overall PL intensity increases because of the suppression of

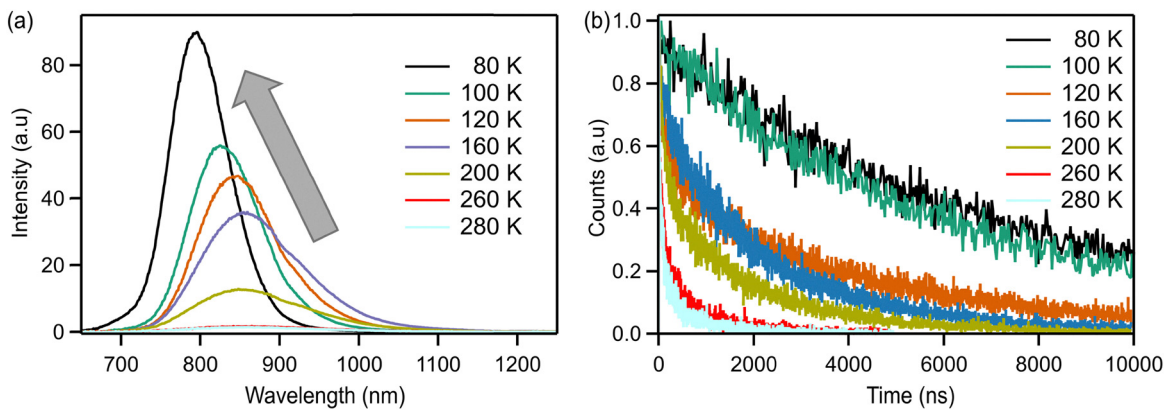

Fig. 4 (a) Temperature-dependent PL spectra of $Au_{18}(DMBT)_{14}$ in 2-MeTHF. (b) TCSPC-measured PL kinetics of $Au_{18}(DMBT)_{14}$ in 2-MeTHF at different temperatures excited at 450 nm (~100 ps pulse).

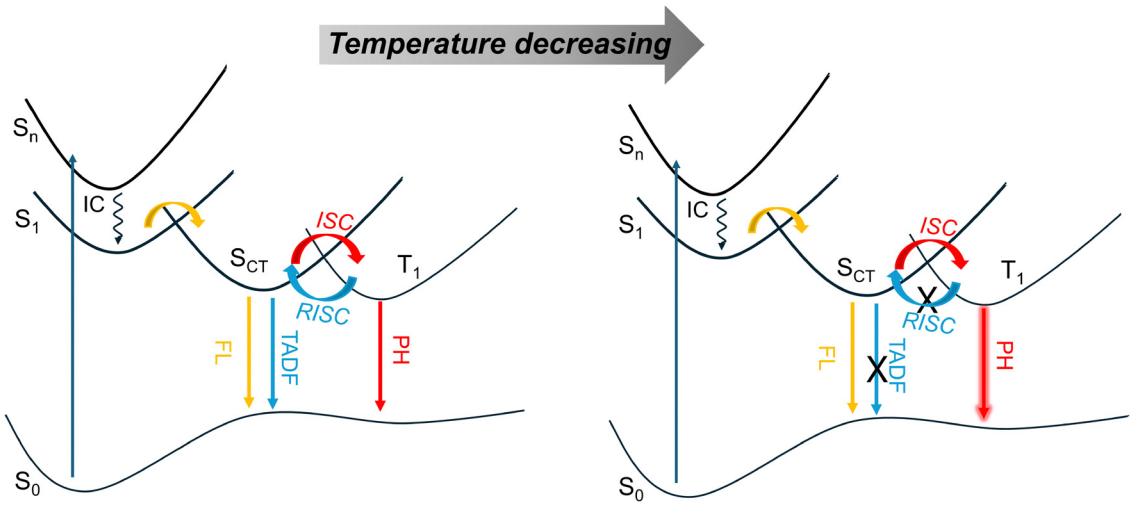

Fig. 5 Proposed excited-state dynamics of $Au_{18}(DMBT)_{14}$ and the temperature effect, where IC = internal conversion, FL = (prompt) fluorescence from $S_{(CT)}$, PH = phosphorescence from T_1, TADF = thermally activated delayed fluorescence *via* reverse ISC.

nonradiative relaxation. The RISC process is fully suppressed when the temperature is lower than 120 K. Thus, only phosphorescence remains.

Conclusions

In summary, the ligand effects on the luminescence of different thiolate-protected NCs have been studied in the isostructural $Au_{18}(SR)_{14}$ NCs protected by aromatic DMBT *vs.* nonaromatic CHT. The study on the excited-state dynamics indicates that $Au_{18}(DMBT)_{14}$ has a relatively larger triplet state population compared to $Au_{18}(CHT)_{14}$ (its triplet state barely observable), consistent with their different lifetime components. This work presents a clear example that the excited states of gold NCs can be modulated by tailoring the types of thiolate ligands, with the aromatic ligands exerting a large influence on the excited state dynamics and pathways owing to the networking interactions among the surface ligands. Future work may extend the investigation to other NCs, such as $Au_{18}(SR)_8(SbPh_3)_4Br_2$ protected by mixed ligands.[67] We expect that the obtained mechanistic insights will provide new perspectives for the future design of metal NCs for applications in photonics, bio-imaging, and other areas.

Data availability

All data are available and are presented in the manuscript and its ESI.†

Conflicts of interest

There are no conflicts to declare.

Acknowledgements

R. J. acknowledges the financial support from the NSF (DMR-2419539).

References

1 Y. Li, M. Zhou, Y. Song, T. Higaki, H. Wang and R. Jin, *Nature*, 2021, **594**, 380–384.
2 S. Takano and T. Tsukuda, *J. Am. Chem. Soc.*, 2021, **143**, 1683–1698.
3 R. Jin, C. Zeng, M. Zhou and Y. Chen, *Chem. Rev.*, 2016, **116**, 10346–10413.
4 M. Zhou, T. Higaki, G. Hu, M. Y. Sfeir, Y. Chen, D. Jiang and R. Jin, *Science*, 2019, **364**, 279–282.
5 Y. Pei and X. Cheng Zeng, *Nanoscale*, 2012, **4**, 4054–4072.
6 E. Khatun, M. Bodiuzzaman, K. S. Sugi, P. Chakraborty, G. Paramasivam, W. A. Dar, T. Ahuja, S. Antharjanam and T. Pradeep, *ACS Nano*, 2019, **13**, 5753–5759.
7 S. M. van de Looij, E. R. Hebels, M. Viola, M. Hembury, S. Oliveira and T. Vermonden, *Bioconjugate Chem.*, 2022, **33**, 4–23.
8 L.-Y. Chen, C.-W. Wang, Z. Yuan and H.-T. Chang, *Anal. Chem.*, 2015, **87**, 216–229.
9 M. A. Abbas, T. Kim, S. U. Lee, Y. S. Kang and J. H. Bang, *J. Am. Chem. Soc.*, 2016, **138**, 390–401.
10 H. Yuan, I. Russier-Antoine, C. Moulin, P.-F. Brevet, Ž. S. Maršić, M. P. Bakulić, X. Kang, R. Antoine and M. Zhu, *Nanoscale Horiz.*, 2025, **10**, 314–321.
11 J. S. A. Devi, S. M. Anju, G. M. Lekha, R. S. Aparna and S. George, *Nanoscale Horiz.*, 2024, **9**, 1683–1702.
12 Y. Du, C. Li, Y. Dai, H. Yin and M. Zhu, *Nanoscale Horiz.*, 2024, **9**, 1262–1278.
13 S. Maity, S. Kolay, S. Chakraborty, A. Devi, Rashi and A. Patra, *Chem. Soc. Rev.*, 2025, **54**, 1785–1844.
14 Z. Liu, L. Luo and R. Jin, *Adv. Mater.*, 2024, **36**, 2309073.
15 K. Tan, H. Ma, X. Mu, Z. Wang, Q. Wang, H. Wang and X.-D. Zhang, *Anal. Bioanal. Chem.*, 2024, **416**, 5871–5891.
16 Y. Chen, M. Zhou, Q. Li, H. Gronlund and R. Jin, *Chem. Sci.*, 2020, **11**, 8176–8183.
17 L. Luo, Z. Liu, X. Du and R. Jin, *Commun. Chem.*, 2023, **6**, 1–6.
18 P. Mastracco, A. Gonzàlez-Rosell, J. Evans, P. Bogdanov and S. M. Copp, *ACS Nano*, 2022, **16**, 16322–16331.

19 M. P. Maman, A. S. Nair, H. Cheraparambil, B. Pathak and S. Mandal, *J. Phys. Chem. Lett.*, 2020, **11**, 1781–1788.
20 L. Luo, Z. Liu, X. Du and R. Jin, *J. Am. Chem. Soc.*, 2022, **144**, 19243–19247.
21 L. Luo, Z. Liu, J. Kong, C. G. Gianopoulos, I. Coburn, K. Kirschbaum, M. Zhou and R. Jin, *Proc. Natl. Acad. Sci. U. S. A.*, 2024, **121**, e2318537121.
22 Q. Li, C. J. Zeman IV, Z. Ma, G. C. Schatz and X. W. Gu, *Small*, 2021, **17**, 2007992.
23 Z. Wu and R. Jin, *Nano Lett.*, 2010, **10**, 2568–2573.
24 W.-Q. Shi, L. Zeng, R.-L. He, X.-S. Han, Z.-J. Guan, M. Zhou and Q.-M. Wang, *Science*, 2024, **383**, 326–330.
25 M. Mitsui, D. Arima, Y. Kobayashi, E. Lee and Y. Niihori, *Adv. Opt. Mater.*, 2022, **10**, 2200864.
26 W.-D. Si, C. Zhang, M. Zhou, W.-D. Tian, Z. Wang, Q. Hu, K.-P. Song, L. Feng, X.-Q. Huang, Z.-Y. Gao, C.-H. Tung and D. Sun, *Sci. Adv.*, 2023, **9**, eadg3587.
27 Y. Wang, C. G. Gianopoulos, Z. Liu, K. Kirschbaum, D. Alfonso, D. R. Kauffman and R. Jin, *JACS Au*, 2024, **4**, 1928–1934.
28 H. Hirai, S. Takano, T. Nakashima, T. Iwasa, T. Taketsugu and T. Tsukuda, *Angew. Chem., Int. Ed.*, 2022, **61**, e202207290.
29 S. Wang, X. Meng, A. Das, T. Li, Y. Song, T. Cao, X. Zhu, M. Zhu and R. Jin, *Angew. Chem., Int. Ed.*, 2014, **53**, 2376–2380.
30 N. L. Smith and K. L. Jr. Knappenberger, *J. Phys. Chem. A*, 2024, **128**, 7620–7627.
31 X.-Y. Xie, K.-Q. Cheng, W.-K. Chen, W. Li, Q. Li, J. Han, W.-H. Fang and G. Cui, *J. Phys. Chem. Lett.*, 2023, **14**, 10025–10031.
32 W. Fan, Y. Yang, Q. You, J. Li, H. Deng, N. Yan and Z. Wu, *J. Phys. Chem. C*, 2023, **127**, 816–823.
33 X. Yu, Y. Sun, W. Xu, J. Fan, J. Gao, X. Jiang, Y. Su and J. Zhao, *Nanoscale Horiz.*, 2022, **7**, 1192–1200.
34 S.-H. Cha, J.-U. Kim, K.-H. Kim and J.-C. Lee, *Chem. Mater.*, 2007, **19**, 6297–6303.
35 G. Soldan, M. A. Aljuhani, M. S. Bootharaju, L. G. AbdulHalim, M. R. Parida, A.-H. Emwas, O. F. Mohammed and O. M. Bakr, *Angew. Chem., Int. Ed.*, 2016, **55**, 5749–5753.
36 Q. Li, C. J. I. Zeman, G. C. Schatz and X. W. Gu, *ACS Nano*, 2021, **15**, 16095–16105.
37 W.-D. Si, C. Zhang, M. Zhou, Z. Wang, L. Feng, C.-H. Tung and D. Sun, *Sci. Adv.*, 2024, **10**, eadm6928.
38 K. Mutoh, T. Yahagi, S. Takano, S. Kawakita, T. Iwasa, T. Taketsugu, T. Tsukuda and T. Nakashima, *Chem. Sci.*, 2025, **16**, 8240–8246.
39 K. Li, P. Wang and Y. Pei, *J. Phys. Chem. Lett.*, 2024, **15**, 9216–9225.
40 M. S. Devadas, J. Kim, E. Sinn, D. Lee, T. I. Goodson and G. Ramakrishna, *J. Phys. Chem. C*, 2010, **114**, 22417–22423.
41 M. S. Devadas, V. D. Thanthirige, S. Bairu, E. Sinn and G. Ramakrishna, *J. Phys. Chem. C*, 2013, **117**, 23155–23161.
42 H. Qian, M. Y. Sfeir and R. Jin, *J. Phys. Chem. C*, 2010, **114**, 19935–19940.
43 T. D. Green and K. L. Knappenberger, *Nanoscale*, 2012, **4**, 4111–4118.
44 T. Stoll, E. Sgrò, J. W. Jarrett, J. Réhault, A. Oriana, L. Sala, F. Branchi, G. Cerullo and K. L. Knappenberger, *J. Am. Chem. Soc.*, 2016, **138**, 1788–1791.
45 K. L. D. M. Weerawardene and C. M. Aikens, *J. Am. Chem. Soc.*, 2016, **138**, 11202–11210.
46 A. Mazumder, K. Li, Z. Liu, Y. Wang, Y. Pei, L. A. Peteanu and R. Jin, *ACS Nano*, 2024, **18**, 21534–21543.
47 X.-K. Wan, J.-Q. Wang, Z.-A. Nan and Q.-M. Wang, *Sci. Adv.*, 2017, **3**, e1701823.
48 Y. Wang, Z. Liu, A. Mazumder, C. G. Gianopoulos, K. Kirschbaum, L. A. Peteanu and R. Jin, *J. Am. Chem. Soc.*, 2023, **145**, 26328–26338.
49 S. Ito, S. Takano and T. Tsukuda, *J. Phys. Chem. Lett.*, 2019, **10**, 6892–6896.
50 W.-Q. Shi, L. Zeng, Z.-C. Long, Z.-J. Guan, X.-S. Han, F. Hu, M. Zhou and Q.-M. Wang, *J. Phys. Chem. Lett.*, 2025, 2204–2211.
51 Z. Liu, Y. Wang, W. Ji, X. Ma, C. G. Gianopoulos, S. Calderon, T. Ma, L. Luo, A. Mazumder, K. Kirschbaum, E. C. Dickey, L. A. Peteanu, D. Alfonso and R. Jin, *ACS Nano*, 2025, **19**, 9121–9131.
52 G. Yousefalizadeh and K. G. Stamplecoskie, *J. Phys. Chem. A*, 2018, **122**, 7014–7022.
53 A. Ghosh, T. Udayabhaskararao and T. Pradeep, *J. Phys. Chem. Lett.*, 2012, **3**, 1997–2002.
54 Q. Yao, Y. Yu, X. Yuan, Y. Yu, J. P. Xie and J. Y. Lee, *Small*, 2013, **9**, 2696–2701.
55 X.-H. Liu, Y. He, Z. Li, A.-H. Cheng, Z. Song, Z.-X. Yu, S. Chai, C. Cheng and C. He, *J. Colloid Interface Sci.*, 2023, **651**, 368–375.
56 R. Itteboina, U. D. Madhuri, P. Ghosal, M. Kannan, T. K. Sau, T. Tsukuda and S. Bhardwaj, *J. Phys. Chem. A*, 2018, **122**, 1228–1234.
57 M. Hesari and Z. Ding, *Chem. – Eur. J.*, 2021, **27**, 14821–14825.
58 M. K. Veedu, J. Osmólska, A. Hajda, J. Olesiak-Banska and J. Wenger, *Nanoscale Adv.*, 2024, **6**, 570–577.
59 A. Das, C. Liu, H. Y. Byun, K. Nobusada, S. Zhao, N. Rosi and R. Jin, *Angew. Chem., Int. Ed.*, 2015, **54**, 3140–3144.
60 S. Chen, S. Wang, J. Zhong, Y. Song, J. Zhang, H. Sheng, Y. Pei and M. Zhu, *Angew. Chem., Int. Ed.*, 2015, **54**, 3145–3149.
61 Q. Yao, L. Liu, S. Malola, M. Ge, H. Xu, Z. Wu, T. Chen, Y. Cao, M. F. Matus, A. Pihlajamäki, Y. Han, H. Häkkinen and J. Xie, *Nat. Chem.*, 2023, **15**, 230–239.
62 A. Tlahuice-Flores, *Phys. Chem. Chem. Phys.*, 2016, **18**, 27738–27744.
63 S. Havenridge and C. M. Aikens, *J. Phys. Chem. A*, 2023, **127**, 9932–9943.
64 K. G. Stamplecoskie, Y.-S. Chen and P. V. Kamat, *J. Phys. Chem. C*, 2014, **118**, 1370–1376.
65 M. Mitsui, *J. Phys. Chem. Lett.*, 2024, **15**, 12257–12268.
66 M. Zhou, C. Zeng, M. Y. Sfeir, M. Cotlet, K. Iida, K. Nobusada and R. Jin, *J. Phys. Chem. Lett.*, 2017, **8**, 4023–4030.
67 J. B. Patty, S. Havenridge, D. Tietje-Mckinney, M. A. Siegler, K. K. Singh, R. H. Hosseini, M. Ghabin, C. M. Aikens and A. Das, *J. Am. Chem. Soc.*, 2022, **144**, 478–484.

